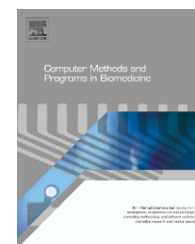




ELSEVIER

journal homepage: www.intl.elsevierhealth.com/journals/cmpb

A wavelet-based Markov random field segmentation model in segmenting microarray experiments

Emmanouil Athanasiadis^{a,*}, Dionisis Cavouras^b, Spyros Kostopoulos^b,
Dimitris Glotsos^b, Ioannis Kalatzis^b, George Nikiforidis^a

^a Medical Image Processing and Analysis (M.I.P.A.) Group, Laboratory of Medical Physics, School of Medical Science, University of Patras, 26 500 Rion - Patras, Greece

^b Medical Image and Signal Processing (MED.I.S.P.) Laboratory, Department of Medical Instruments Technology, Technological Educational Institute of Athens, Ag. Spyridonos Street, Aigaleo, 122 10, Athens, Greece

ARTICLE INFO

Article history:

Received 5 May 2010

Received in revised form

17 February 2011

Accepted 11 March 2011

Keywords:

cDNA microarray

Markov Random Field (MRF)

Image segmentation

Wavelet

ABSTRACT

In the present study, an adaptation of the Markov Random Field (MRF) segmentation model, by means of the stationary wavelet transform (SWT), applied to complementary DNA (cDNA) microarray images is proposed (WMRF). A 3-level decomposition scheme of the initial microarray image was performed, followed by a soft thresholding filtering technique. With the inverse process, a Denoised image was created. In addition, by using the Amplitudes of the filtered wavelet Horizontal and Vertical images at each level, three different Magnitudes were formed. These images were combined with the Denoised one to create the proposed SMRF segmentation model. For numerical evaluation of the segmentation accuracy, the segmentation matching factor (SMF), the Coefficient of Determination (r^2), and the concordance correlation (p_c) were calculated on the simulated images. In addition, the SMRF performance was contrasted to the Fuzzy C Means (FCM), Gaussian Mixture Models (GMM), Fuzzy GMM (FGMM), and the conventional MRF techniques. Indirect accuracy performances were also tested on the experimental images by means of the Mean Absolute Error (MAE) and the Coefficient of Variation (CV). In the latter case, SPOT and SCANALYZE software results were also tested. In the former case, SMRF attained the best SMF, r^2 , and p_c (92.66%, 0.923, and 0.88, respectively) scores, whereas, in the latter case scored MAE and CV, 497 and 0.88, respectively. The results support the performance superiority of the SMRF algorithm in segmenting cDNA images.

© 2011 Elsevier Ireland Ltd. All rights reserved.

1. Introduction

In the last decay, complementary DNA (cDNA) microarray technology has been enormously improved, by offering to the research community the ability to identify and quantify thousands of genes simultaneously [1]. cDNA microarrays consist of thousands of individual DNA sequences placed on a dif-

ferent microscope slide spot on the microarray. Messenger RNA (mRNA) from a sample and a reference cell is collected and reverse transcribed into cDNA sequence [1]. Each of the two cDNA samples is labeled using two different fluorescence dyes, green Cyanine 3 (Cy3), for the reference, and red, Cyanine 5 (Cy5), for the control sample. These two samples are mixed and hybridized with the microarray slide. After this hybridization, the slide is scanned and two different images

* Corresponding author. Tel.: +30 2105385375; fax: +30 2105385303.

E-mail address: mathan@upatras.gr (E. Athanasiadis).

0169-2607/\$ – see front matter © 2011 Elsevier Ireland Ltd. All rights reserved.

doi:10.1016/j.cmpb.2011.03.007

(Red and Green) are produced. For each spot that corresponds to a specific gene, the fluorescence ratio of the red versus green channel is indicative of the expression level of the corresponding gene in the two samples (control vs. reference). Hence, the more precise the localization of a spot on the arrayer, the more accurate the intensity measurement is and, consequently, a more precise expression level measurement of the gene may be obtained. Therefore, the exact location, as well as, an accurate identification of the boundary of each spot is crucial for more precise gene expression measurements.

According to the literature, there are three major steps employed for the calculation of the expression level of each gene in the cDNA image [1,2]. The first step is the gridding step, where the precise localization of each spot with each background area is defined. The second step is the segmentation [3-8], where the classification of the pixel to either the foreground or the background of the image-spot is performed. The final step is the intensity extraction step, where the intensity of each spot is calculated.

In the present study, the gridding step is assumed to have been done by means of an automatic gridding process, previously developed by our group [10], thus, we will focus on the segmentation process. More precisely, a new segmentation algorithm is proposed based on the MRF model in combination with the additional information given by the wavelet domain [12] of the microarray image. The Stationary Wavelet Transform is used to decompose the image up to 3 scales, followed by a soft thresholding filter [11]. SWT was selected due to the fact that decomposed images retain their initial dimensions and no loss of information occurs. Magnitude images from each one of the three scales, combined with the wavelet filtered image are used to enhance the segmentation accuracy of the proposed wavelet-based MRF scheme.

2. Methods

2.1. Material

An indirect performance estimation of the segmentation algorithms was also carried out, with the use of five actual microarray images concerning *Saccharomyces cerevisiae* [16]. More precisely, 10 images (5 Red and 5 Green) from the same experiment, produced at five different time intervals [16], were employed. Common reference channel (Green) intensities were considered constant in time [17]. This property was used to examine the reproducibility of each segmentation algorithm [17] and the algorithm with the more stable results would be the most effective.

In addition, the use of simulated microarray images is essential for the task of directly calculating the segmentation accuracy of the algorithms, due to the fact that the numerical evaluation of the segmentation accuracy is not a straight forward process since the actual boundaries of the spots cannot be accurately defined. Thus, a simulated microarray image with 1600 spots was produced, according to [12]. More specifically, an actual microarray image with 1600 spots was converted into binary image by means of simple thresholding filtering. This binary image was used as a template in order to create the simulated image with realistic characteristics. Each

spot (foreground) was filled with intensity values, randomly chosen by an exponential distribution with predefined mean value ranging from 0 to $2^{16} - 1$. The background was filled with intensity values randomly chosen by a single exponential distribution with mean value equal to 4000. Afterward, the image was corrupted with additive Gaussian noise [9] of five different Signal to Noise Ratio (SNR) levels, 1, 3, 5, 7, and 9 db. These five images would be used for directly evaluating the segmentation performance of the algorithms at different noise levels.

2.2. Proposed Wavelet MRF (WMRF) Model

The WMRF models make use of both textural and contextual information of the image [12,14,18], and [19]. In order to use additional useful information residing on the microarray image, the stationary wavelet transform [18] was applied onto the image up to scale three followed by a soft threshold filtering technique, as described in (1)

$$W_{out} = \begin{cases} W_{in} + Th \cdot (G - 1) & \text{if } W_{in} > Th \\ W_{in} - Th \cdot (G - 1) & \text{if } W_{in} < -Th \\ G \cdot W_{in} & \text{otherwise} \end{cases} \quad (1)$$

where W_{out} and W_{in} are considered to be the output and the input wavelet domain values of the image, and Th and G are the threshold and gain values, respectively. Filtering is applied to all wavelet domain detail images; Horizontal (H_o), Vertical (V_e) and Diagonal (D_i). Following a trial and error procedure, the biorthogonal mother wavelet [19] was chosen. The whole process is illustrated in Fig. 1.

The denoised image (D) as well as the three magnitude images (M_1 , M_2 , and M_3) [15] in relation (2) for each scale were formed

$$M = \sqrt{H_o^2 + V_e^2} \quad (2)$$

where H_o and V_e are the Horizontal and the Vertical filtered wavelet detail images at the 1st, 2nd and 3rd scale, respectively.

Assuming that a feature vector F has been extracted from a random image X and that the segmentation result ("0" label for the Background and "1" for the spot) is a binary vector Y , then according to Bayesian theory, the a-posteriori probability $P(Y|F)$ of Y given the F can be derived from (3), known as Bayes' Rule.

$$P(Y|F) \cong p(F|Y)P(Y) \quad (3)$$

where $p(F|Y)$ is the conditional probability of F given the Y , and $P(Y)$ is the a priori probability of Y that is used to describe the label distribution. The a-posteriori probability can also be expressed using Gibbs' distribution [12] as shown in (4).

$$P(Y|F) = \frac{1}{Z} e^{-SE^C/T} \quad (4)$$

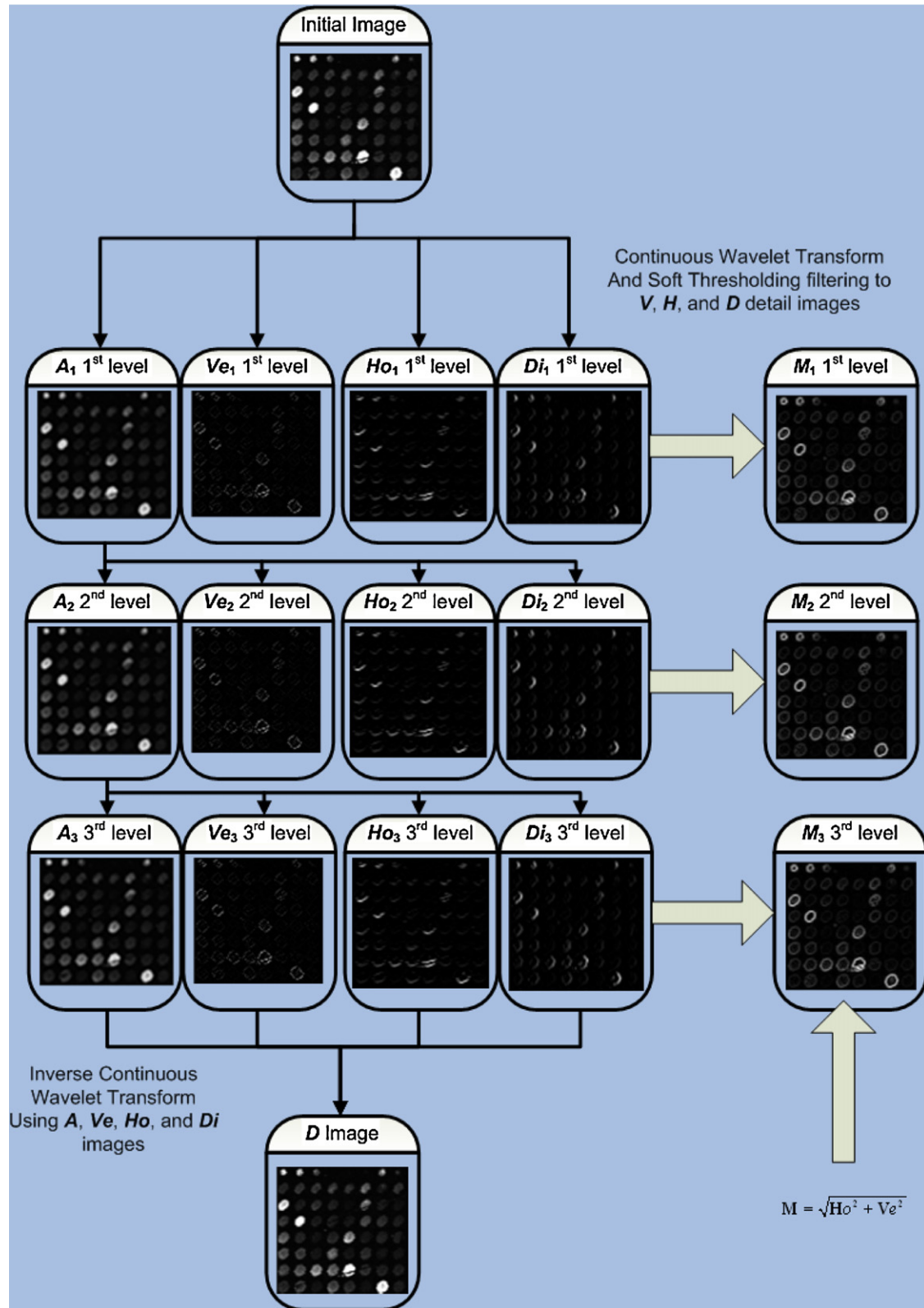


Fig. 1 - Wavelet decomposition and image formation scheme.

where Z is normalization constant calculated by (5), SE^c is the total energy for each class c , calculated by (6) and T is a constant value.

$$Z = \sum_{c=1}^2 e^{-SE^c/T} \quad (5)$$

$$SE^c = SE_L + aSE_F^c \quad (6)$$

where SE_L and SE_F are the energy of the labels (7) and features (8), respectively, and a is a normalization value.

$$SE_L(y) = w_1 \sum_{t \in Neighbor} \delta(y_t, y_{center})_D + w_2 \sum_{i=1}^L \left[\sum_{t \in Neighbor} \delta(y_t, y_{center})_{M_i} \right] \quad (7)$$

$$SE_F^c = w_1 \left[\frac{(D - \mu_D^c)^2}{2(\sigma_D^c)^2} + \log(\sqrt{2\pi}\sigma_D^c) \right] + w_2 \sum_{i=1}^L \left\{ \left[\frac{(M_i - \mu_{M_i}^c)^2}{2(\sigma_{M_i}^c)^2} + \log(\sqrt{2\pi}\sigma_{M_i}^c) \right] \right\} \quad (8)$$

where μ_D and μ_{M_i} are the mean values of class c of smoothed magnitude images M and denoised image D , respectively, and L is the maximum level of decomposition (i.e. 3). Finally, σ_D and σ_{M_i} are the standard deviations of M and D images of class c , respectively. W_1 and $W_2 \in [0, 1]$ are weight parameters.

For the calculation of the a-posteriori probability $P(Y|F)$ in (1), the following scheme was followed:

- For each spot with its background, the fuzzy c means clustering algorithm [18] was used for an initial estimation of the 2 classes C , the foreground (spot) and background classes.
- For each class C , mean value μ and standard deviation σ were calculated.
- The SE_L and two SE_F^c (one for each class C) energies were calculated by using (7) and (8), respectively.
- Total Energies (4) for each class C were calculated.
- A-posteriori probabilities (2) of each pixel belonging to either foreground, or background were calculated. Classification was performed to the highest probability.
- Label values of vector Y were redefined according to the classification decision.
- The whole process was repeated until no significant change of the total energies SE^c occurred.

2.3. Intensity extraction and normalization

Regarding simulated images, for each segmented spot, the mean intensity value of the foreground (I_{FG}) and the background (I_{BG}) was calculated. The spot intensity value I was calculated by subtracting I_{FG} from I_{BG} (background correction) [17]. Regarding the actual microarray images, background correction was applied to both Red and Green Channels. In the latter case, in order to adjust individual intensities among the five replicates, normalisation was an essential step. As discussed in the literature [1], with normalization process, elimination of the biases within each microarray involved in

an experiment is achieved, thus, microarray data can be used for further analysis

In the present study, the local weighted linear regression (lowess) [17] method was adopted. According to this method, IR plots ($I = \log_{10}(R/G)$ and $R = \log_2(R/G)$) were formed, where R and G are the red and green channel's mean spot intensity values. Afterwards, normalization was accomplished with the use of a best-fit weighted function on the IR plot. More detail about lowess normalization method can be found in [17]

2.4. Evaluation

In order to make a direct assessment of the segmentation process, the following metrics were calculated from the simulated images:

- The segmentation matching factor (SMF) [13,20] that measures the mis-segmented pixels.

$$SMF = \frac{B_{segmented} \cap B_{simulated}}{B_{segmented} \cup B_{simulated}} \quad (9)$$

where $B_{segmented}$ and $B_{simulated}$ are the binary versions of the segmented and simulated images, respectively.

The algorithm that scored an SMF value closest to unity had the best performance.

- The coefficient of determination r^2 [13,20] indicates the strength of the linear association between simulated and calculated cells, as well as, it gives the proportion of the variance (fluctuation) of the calculated data.

$$r^2 = \frac{\sum_{i=1}^{All \ spots} (I_{segmented(i)} - \bar{I}_{actual})^2}{\sum_{i=1}^{All \ spots} (I_{actual(i)} - \bar{I}_{actual})^2} \quad (10)$$

where $I_{segmented}$ and I_{actual} are the mean intensity values of the calculated and simulated spots, respectively, i refers to individual cell images ($i = 1 \dots 1600$), and \bar{I}_{actual} is the overall mean of the spot intensity values of the simulated image. The algorithm that scores r^2 value closest to the unity has the best performance.

- The concordance correlation p_c [13,20] measures the agreement between simulated and calculated data and is used to evaluate the reproducibility of the proposed segmentation algorithms.

$$p_c(A, B) = \frac{2S_A S_B r}{S_A^2 + S_B^2 + (\bar{A} - \bar{B})^2} \quad (11)$$

where A and B are two samples, \bar{A} and \bar{B} are the mean values, S_A and S_B are the standard deviation of the samples. The higher the p_c value, the better the performance of the algorithm.

Indirect segmentation performance estimation was made with the use of the real microarray images, where the reproducibility of the segmentation techniques was quantified by means of:

- Mean Absolute Error (MAE) [20] that indicates the sameness of the spots' intensities.

$$MAE_{spot} = \frac{1}{n} \sum_{i=1}^n |I_i - \bar{I}| \quad (12)$$

where n is the number of replicates ($n=5$), I_i is the normalized mean spot intensity value and \bar{I} is the spot's overall mean, calculated from the means of the corresponding spots in the n replicates.

- Coefficient of Variation (CV) [20] that indicates the variations of the spots' intensities.

$$CV_{spot} = \frac{\sigma}{\mu} \quad (13)$$

The lower the MAE and the CV values, the better is the reproducibility of the method being evaluated.

For segmentation accuracy comparison purposes, MRF, and the proposed WMRF algorithms were compared against the conventional fuzzy c means (FCM) [19], the Gaussian Mixture Models (GMM) and the Fuzzy Gaussian Mixture Models (FGMM) that have been developed and applied to microarray images by our group in the past and explicitly described at [20]. The SMF, the r^2 , and the p_c were used for the evaluation of segmentation's algorithms, since the former concerns segmentation accuracy and the two latter intensity extraction precision.

3. Results

Comparative segmentation results for 6 different cells, obtained from the G channel of the simulated microarrays, are presented in Table 1. The first column indicates the simulated spot with the surrounding area, the second column indicates the actual boundaries of the spot and the third, fourth, fifth, and sixth columns present the segmentation results as well as the corresponding SMF of the GMM (87.60%, 95.87%, 91.74%, 95.87%, 89.26%, 95.04%), FGMM (100%, 97.52%, 100%, 96.69%, 100%, 98.35%), MRF (98.35%, 96.69%, 100%, 96.69%, 100%, 98.35%), and WMRF (100%, 98.35%, 100%, 98.35%, 100%, 100%) algorithms, respectively. Results concerning SMF, r^2 , and p_c on simulated images at five different SNR levels applied to FCM, GMM, FGMM, the conventional MRF, and the proposed WMRF technique are illustrated in Tables 2–4 and Figs. 2–4, respectively.

Furthermore, GMM, FGMM, MRF and WMRF algorithms were also used to segment five experimental microarray images. Green channel intensity was expected to be constant in time during the experiment's progression [19], and [20]. Thus, for the performance assessment of the above algorithms, reproducibility (MAE and CV) of the resulting spot intensity values on the green channel was calculated and presented in Table 5. Furthermore, normalized box-plots that illustrate the MAE using GMM (1470), FGMM (1430), MRF (1215), WMRF (497), SPOT (1180) and SCANALYZE (503), applied on the five real microarray images, are illustrated in Fig. 5.

4. Discussion

In this study, we propose a novel generalised wavelet-based MRF (WMRF) segmentation model in segmenting microarray images. The main novelty of the WMRF technique is that it takes into account the spatial information of the pixels in the wavelet domain, during the process of label calculation of the MRF model, leading to a more robust and accurate pixel classification procedure. The latter is verified by the results obtained by applying the proposed algorithm to both simulated and actual microarray images.

More precisely, concerning simulated images, the proposed WMRF algorithm attained the highest SMF, r^2 , and p_c scores (see Tables 1–4 and Figs. 2–4, respectively) as compared to the FCM, GMM, FGMM, and the conventional MRF technique, at all five different SNR levels. Segmentation results on simulated images of six randomly chosen spots are also illustrated in Table 1. In particular, in the case of the SMF at the 1db SNR Gaussian noise level (see Table 2), the FCM scored 89.22% whereas the GMM and the FGMM scored 90.73% and 91.07%, and the MRF and WMRF scored 92.15% and 92.66%, respectively. The SMF difference between the FCM and SMRF was found constant at different SNR levels. On the contrary, r^2 variations among FCM, GMM, FGMM, MRF, and SMRF were diminished for higher SNR levels (see Table 3). Comparing the two GMM algorithms, the Fuzzy approach of the GMM was more tolerant to noise as compared to the conventional GMM. In addition, the SMRF segmentation performance was superior to the conventional MRF algorithm.

In addition, GMM, FGMM, MRF and WMRF algorithms were applied to five experimental microarray images. The segmentation performance was accomplished by means of two metrics, the MAE (sameness) and the CV (variation). In addition, a comparison with the publicly available software programs SCANALYZE[®] and SPOT[®] was conducted for segmenting the same microarray images; the SCANALYZE software makes use of the Fixed Circle (FC) segmentation technique and SPOT of the SRG.

The lowest MAE and CV measurements were obtained by the proposed WMRF method. More precisely, WMRF scored 497 mean MAE for the 6400 spots (see Table 5 and Fig. 5), which is close to the score attained by the FC technique.

Additionally, the MAE of the proposed WMRF technique was half that of the conventional MRF, which is indicative of the improvement on MRF that wavelet based information may bring about. Additionally, the proposed method achieved a MAE (497) score lower but close to SCANALYZE's FC technique (503) but definitely lower than that of the conventional MRF technique (1215) and of the SPOT's SRG technique (1180). Additionally, the CV values of WMRF, FC, SRG, and MRF (0.88, 0.90, 0.93, and 1.15, respectively) were close to unity with the WMRF having the lowest value

The WMRF algorithm results on the real microarray images verify the simulated results and support the performance superiority of the WMRF algorithm in segmenting cDNA images.

Concerning segmentation processing time for an actual microarray image of 6400 spots, it took around 25 min for the

Table 1 – Comparative results for 6 different cells obtained from the G channel of the simulated microarray. The 1st column indicates the simulated spot with the surrounding area, the 2nd column indicates the actual boundaries of the spot and the 3rd, 4th, 5th, and 6th columns present the segmentation results of the GMM, FGMM, MRF, and WMRF algorithms as well as the corresponding matching factors.







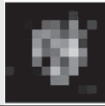




















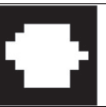
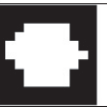
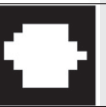
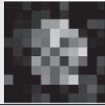





| SEGMENTATION RESULTS FOR 6 DIFFERENT CELLS | | | | | |
|---|---|---|---|---|--|
| Original Spots | Actual Boundaries | GMM Result | FGMM Result | MRF Result | WMRF Result |
|  |  |  |  |  |  |
| Spot 1 | Accuracy: | 87.60% | 100.00% | 98.35% | 100.00% |
|  |  |  |  |  |  |
| Spot 2 | Accuracy: | 95.87% | 97.52% | 96.69% | 98.35% |
|  |  |  |  |  |  |
| Spot 3 | Accuracy: | 91.74% | 100.00% | 100.00% | 100.00% |
|  |  |  |  |  |  |
| Spot 4 | Accuracy: | 95.87% | 96.69% | 96.69% | 98.35% |
|  |  |  |  |  |  |
| Spot 5 | Accuracy: | 89.26% | 100.00% | 100.00% | 100.00% |
|  |  |  |  |  |  |
| Spot 6 | Accuracy: | 95.04% | 98.35% | 98.35% | 100.00% |

Table 2 – Comparative SMF results for the 5 simulated images with different SNR levels. The 2nd, 3rd, 4th, 5th, and 6th columns indicate the SMF by using FCM, GMM, FGMM, MRF and WMRF segmentation techniques, respectively.

| SMF results on simulated microarray images | | | | | |
|--|-------|-------|-------|-------|-------|
| SNR (db) | FCM | GMM | FGMM | MRF | WMRF |
| 1 | 89.22 | 90.73 | 91.07 | 92.15 | 92.66 |
| 3 | 89.94 | 91.59 | 92.50 | 92.96 | 93.53 |
| 5 | 91.25 | 92.20 | 93.84 | 94.24 | 94.56 |
| 7 | 93.11 | 93.39 | 95.48 | 96.30 | 96.69 |
| 9 | 94.69 | 95.34 | 96.62 | 97.20 | 97.47 |

Table 3 – Comparative r^2 results for the 5 simulated images with different SNR levels. The 2nd, 3rd, and 4th columns indicate r^2 by using FCM, MRF and the proposed WMRF segmentation techniques, respectively.

| r^2 results on simulated microarray images | | | | | |
|--|-------|-------|-------|-------|-------|
| SNR (db) | FCM | GMM | FGMM | MRF | WMRF |
| 1 | 0.843 | 0.894 | 0.916 | 0.905 | 0.923 |
| 3 | 0.867 | 0.914 | 0.936 | 0.927 | 0.944 |
| 5 | 0.926 | 0.935 | 0.957 | 0.946 | 0.966 |
| 7 | 0.955 | 0.961 | 0.983 | 0.968 | 0.988 |
| 9 | 0.971 | 0.983 | 0.991 | 0.987 | 0.996 |

Table 4 – Comparative SMF results for the 5 simulated images with different SNR levels. The 2nd, 3rd, 4th, 5th, and 6th columns indicate the SMF by using FCM, GMM, FGMM, MRF and WMRF segmentation techniques, respectively.

| p_c results on simulated microarray images | | | | | |
|--|------|------|------|------|------|
| SNR (db) | FCM | GMM | FGMM | MRF | WMRF |
| 1 | 0.80 | 0.83 | 0.86 | 0.85 | 0.88 |
| 3 | 0.80 | 0.83 | 0.87 | 0.86 | 0.89 |
| 5 | 0.81 | 0.84 | 0.90 | 0.87 | 0.91 |
| 7 | 0.82 | 0.85 | 0.93 | 0.89 | 0.94 |
| 9 | 0.84 | 0.87 | 0.95 | 0.92 | 0.97 |

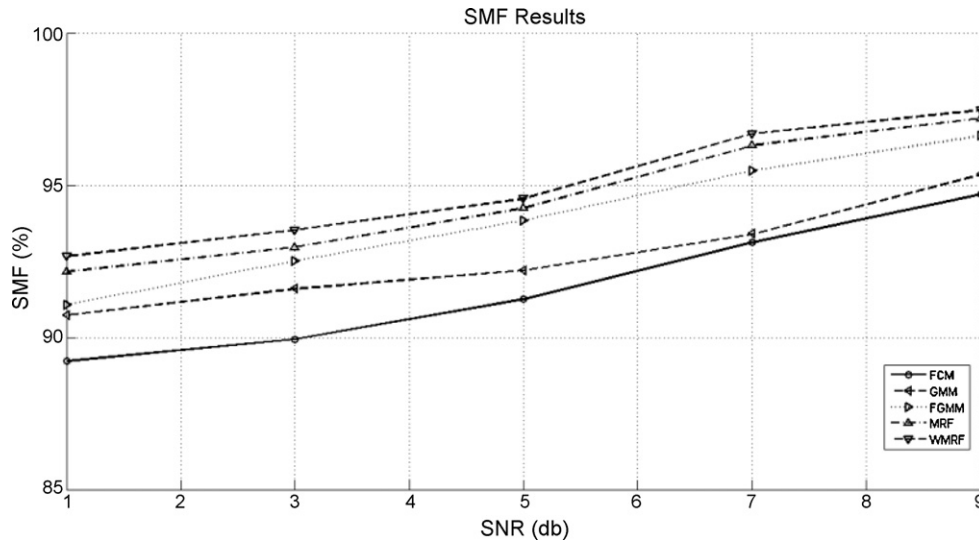


Fig. 2 – SMF calculated by using FCM, GMM, FGMM, MRF, and WMRF algorithms in respect to additive white Gaussian noise with different SNR.

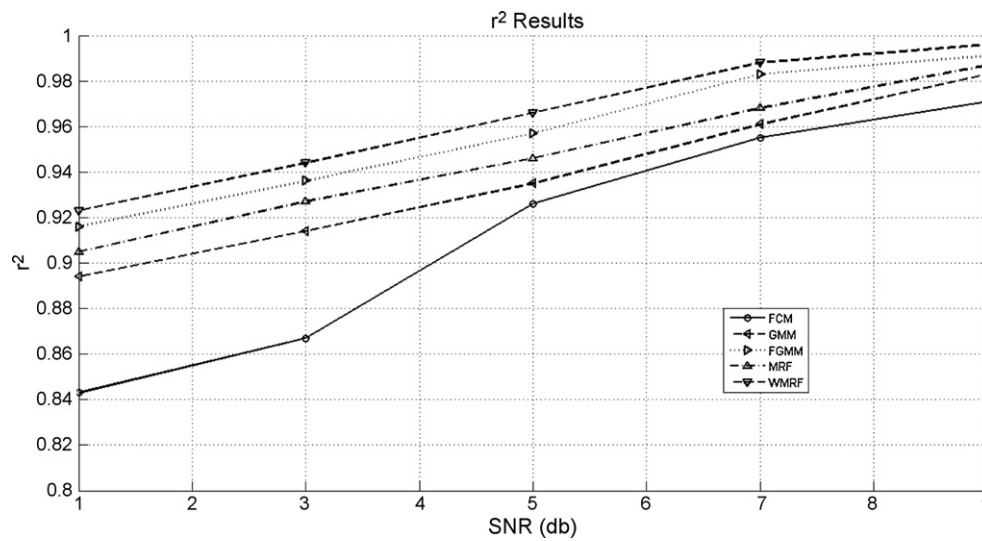


Fig. 3 – r^2 calculated by using FCM, GMM, FGMM, MRF, and WMRF algorithms in respect to additive white Gaussian noise with different SNR.

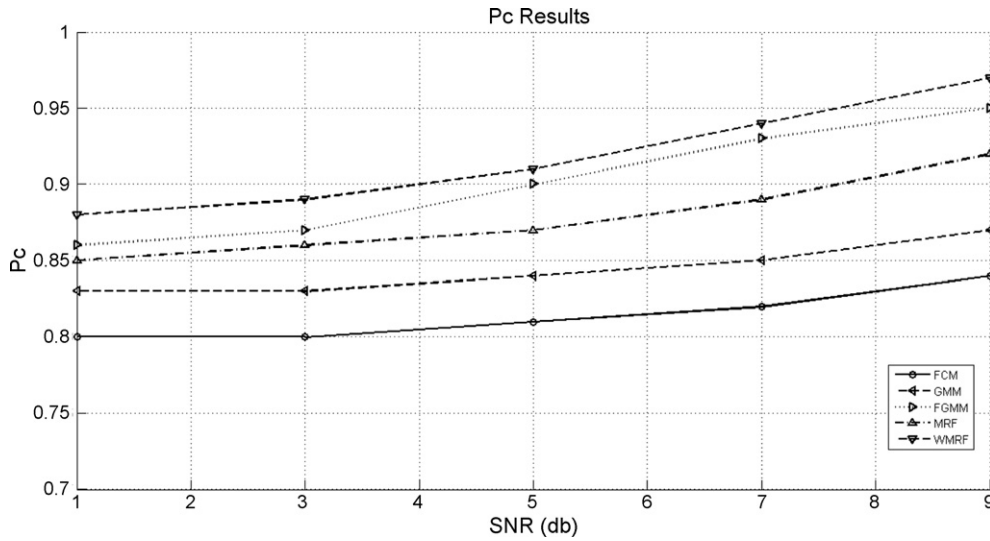


Fig. 4 – p_c calculated by using FCM, GMM, FGMM, MRF, and WMRF algorithms in respect to additive white Gaussian noise with different SNR.

Table 5 – Results for the four segmentation techniques by means of MAE and CV, applied on five real microarray images.

| MAE and CV results on real microarray images | | | |
|--|----------|---------|--|
| Technique | Mean MAE | Mean CV | |
| GMM | 1470 | 1.29 | |
| FGMM | 1430 | 1.21 | |
| MRF | 1215 | 1.15 | |
| WMRF | 497 | 0.88 | |
| SCANALYZE (FC) | 503 | 0.90 | |
| SPOT (SRG) | 1180 | 0.93 | |

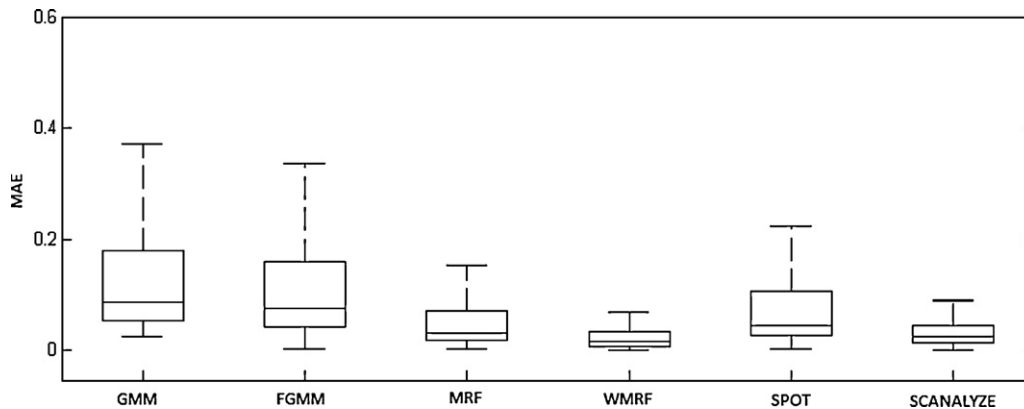


Fig. 5 – Normalized box-plots that illustrate the MAE using GMM, FGMM, MRF, WMRF, SPOT and SCANALYZE applied on five real microarray images.

WMRF, whereas it took 20 min for the conventional MRF, GMM, and FGMM techniques on a Pentium IV 3 GHz desktop PC with 1 GB RAM. However, the programming code of the above algorithms has not been optimized in terms of processing time and, thus, it may not be comparable with SCANALYZE's fast response times.

5. Conclusions

It was found that the proposed method (WMRF), tested on both simulated and actual microarrays, was found to enhance the segmentation accuracy of spots. In addition the proposed

segmentation scheme was contrasted with the conventional MRF, as well as, two publicly available packages, the SPOT and the SCANALYZE. The main reason why the proposed method bestowed better segmentation results was due to the combination of image texture with information given by the image's wavelet domain.

Acknowledgement

We would like to thank the Greek State Scholarships Foundation (IKY) for funding the above work.

REFERENCES

- [1] Y.H. Yang, M.J. Buckley, S. Duboit, T.P. Speed, Comparison of methods for image analysis on cDNA microarray data, *Journal of Computational and Graphical Statistics* 11 (2002) 108–136.
- [2] M. Schena, D. Shalon, R.W. Davis, P.O. Brown, Quantitative monitoring of gene expression patterns with a complementary DNA microarray, *Science* 270 (1995) 467–470.
- [3] M.B. Eisen, ScanAlyze, 1999. Available at: <http://rana.lbl.gov/EisenSoftware.htm>.
- [4] Axon Instruments, Inc., GenPix 4000A User's Guide, 1999.
- [5] GeneSifter Data Center. Available at: <http://www.genesifter.net/web/dataCenter.html>.
- [6] M.J. Buckley, The Spot User's Guide, CSIRO Mathematical and Information Science, 2000. Available at: <http://www.cmis.csiro.au/IAP/Spot/spotmanual.htm>.
- [7] ImaGene, ImaGene 6.1 User Manual. <http://www.biodiscovery.com/index/papps-webfiles-action>.
- [8] R. Adams, L. Bischof, Seeded region growing, *IEEE Transactions on Pattern Analysis and Machine Intelligence* 16 (1994) 641–647.
- [9] K. Blekas, N.P. Galatsanos, I. Georgiou, An unsupervised artifact correction approach for the analysis of DNA microarray images, in: *Proc. IEEE International Conf. on Image Processing (ICIP)*, vol. 2, 2003, pp. 165–168.
- [10] E. Athanasiadis, D. Cavouras, P. Spyridonos, I. Kalatzis, G. Nikiforidis, An automatic microarray image gridding technique based on continuous wavelet transform, *Lecture Notes in Computer Science* 4673 (2007) 854–870.
- [11] J.E. Fowler, The redundant discrete wavelet transform and additive noise, *IEEE Signal Processing Letters* 12 (9) (2005).
- [12] O. Demirkaya, M.H. Asyali, M.M. Shoukri, Segmentation of cDNA microarray spots using Markov random field modeling, *Bioinformatics* 21 (13) (2005) 2994–3000.
- [13] A. Lehmussola, et al., Evaluating the performance of microarray segmentation algorithms, *Bioinformatics* 22 (2006) 2910–2917.
- [14] S. Geman, D. Geman, Stochastic relaxation Gibbs distributions, and the Bayesian restoration of images, *IEEE Transactions on Pattern Analysis and Machine Intelligence* 6 (1984) 721–741.
- [15] P. Sakellariopoulos, L. Costaridou, G. Panayiotakis, A wavelet-based spatially adaptive method for mammographic contrast enhancement, *Physics in Medicine and Biology* 48 (2003) 787–803.
- [16] J.L. DeRisi, V.R. Iyer, P.O. Brown, Exploring the metabolic and genetic control of gene expression on a genomic scale, *Science* 278 (1997) 680.
- [17] Y.H. Yang, S. Dudoit, P. Luu, D.M. Lin, V. Peng, J. Ngai, T.P. Speed, Normalization for cDNA microarray data: a robust composite method addressing single and multiple slide systematic variation, *Nucleic Acid Research* 30 (4) (2002), e15.
- [18] C.S. Burrus, R.A. Gopinath, H. Guo, *Introduction to Wavelets and Wavelet Transforms*, Prentice Hall, Englewood Cliffs, NJ, 1998.
- [19] E.I. Athanasiadis, D.A. Cavouras, D.Th. Glotsos, P.V. Georgiadis, I.K. Kalatzis, G.C. Nikiforidis, Segmentation of complementary DNA microarray images by wavelet-based Markov random field model, in: *IEEE Transaction on Information Technology in Biomedicine*, vol. 13, issue 6, November 2009.
- [20] E.I. Athanasiadis, D.A. Cavouras, P.P. Spyridonos, D.Th. Glotsos, I.K. Kalatzis, G.C. Nikiforidis, Complementary DNA microarray image processing based on the Fuzzy Gaussian mixture model, in: *IEEE Transaction on Information Technology in Biomedicine*, vol. 13, issue 4, July 2009.